LETTER

doi:10.1038/nature12573

Structural insight into magnetochrome-mediated magnetite biomineralization

Marina I. Siponen[1,2,3], Pierre Legrand[4], Marc Widdrat[5], Stephanie R. Jones[6], Wei-Jia Zhang[7,8]†, Michelle C. Y. Chang[6], Damien Faivre[5], Pascal Arnoux[1,2,3,8] & David Pignol[1,2,3,8]

Magnetotactic bacteria align along the Earth's magnetic field using an organelle called the magnetosome, a biomineralized magnetite ($Fe(II)Fe(III)_2O_4$) or greigite ($Fe(II)Fe(III)_2S_4$) crystal embedded in a lipid vesicle. Although the need for both iron(II) and iron(III) is clear, little is known about the biological mechanisms controlling their ratio[1]. Here we present the structure of the magnetosome-associated protein MamP and find that it is built on a unique arrangement of a self-plugged PDZ domain fused to two magnetochrome domains, defining a new class of *c*-type cytochrome exclusively found in magnetotactic bacteria. Mutational analysis, enzyme kinetics, co-crystallization with iron(II) and an *in vitro* MamP-assisted magnetite production assay establish MamP as an iron oxidase that contributes to the formation of iron(III) ferrihydrite eventually required for magnetite crystal growth *in vivo*. These results demonstrate the molecular mechanisms of iron management taking place inside the magnetosome and highlight the role of magnetochrome in iron biomineralization.

Magnetotactic bacteria (MTB) have the particular ability to align with geomagnetic field lines, a phenomenon referred to as magnetotaxis. This magnetotactic property is due to the presence of the magnetosome, an organelle made of a lipid vesicle loaded with a single magnetite or greigite crystal about 50 nm in size. The alignment of magnetosomes inside the cell acts like a compass needle to orient MTB passively in geomagnetic fields, putatively simplifying their search for preferred microaerophilic environments. Formation of this iron-rich organelle is genetically orchestrated by genes located in the magnetosome genetic island. These genes ensure the formation of the vesicles, their alignment, their loading with iron and the biomineralization into magnetite or greigite[2,3]. Despite early observations of redox control in MTB[4,5], this last step remains poorly understood, notably the management of the iron(II) and iron(III) species required for magnetite or greigite formation. There is indication that some oxidized iron species such as ferrihydrite accumulate before magnetite formation, therefore suggesting the need for a reductive process[6,7]. However, there is also growing evidence that the readily available iron species in the magnetosome is iron(II). Both the presence of numerous and active ferric reductases in MTB[8] and the predominance of cation diffusion facilitators for iron(II) trafficking[9] associated with the magnetosome support this premise.

The search for potential redox proteins within the magnetosome genetic island has led to the identification of four gene products containing at least two tandem *c*-type cytochrome motifs CX_2CH, recently called magnetochrome domains[10]: MamE, MamP, MamT and MamX. Among these magnetochrome-containing proteins, MamE and MamP are conserved in all MTB and, interestingly, deletion mutants of the corresponding genes show defects in the biocrystallization process[11,12]. However, the multiplicity of this domain leads to difficulties in the phenotypic analyses of a single-domain deletion mutant in the *mamE* gene[13], suggesting that magnetochrome domains could be functionally redundant. This magnetochrome domain seems specific to MTB as it has not been found in any other species so far, suggesting it may represent a new functional class of cytochrome.

We purified and crystallized the soluble part of MamP from the MO-1 strain (residues 26–260, see Supplementary Methods). The MamP structure was subsequently solved by multi-wavelength anomalous diffraction (MAD) using the four iron atoms present in the asymmetric unit (see Extended Data Table 1 for statistics and Extended Data Fig. 1 for an example of the $2mF_{obs} - DF_{calc}$ map). The first visible residue in the electron density corresponds to residue 87, indicating the presence of a long flexible arm connecting the protein to the single transmembrane helix. Following this flexible arm, the protein folds as a PDZ domain, a small *c*-type cytochrome domain (the first magnetochrome domain, MCR1), a 17-residue linker and finally a second magnetochrome domain (Fig. 1; see Extended Data Fig. 2 for an annotated sequence alignment). The first magnetochrome domain is in contact with its own PDZ domain, whereas the second is projected above the PDZ domain of the other monomer. The minimal unit of MamP is a dimer, although the crystal packing could also support the existence of a tetramer made by two symmetric dimers (one in an 'open' state and the other in a 'closed' state; Extended Data Figs 3 and 4) differing by only small but functionally important side-chain reorientations, as outlined below. In solution, size exclusion chromatography indicates a pH-dependent tetramer/dimer equilibrium that was confirmed by small-angle X-ray scattering (SAXS) whereas circular dichroism measurements indicated no major structural rearrangement upon pH change (Supplementary Methods and Extended Data Fig. 3).

Using the PDZ domain of MamP, a structural homology search using the DALI server[14] indicated that the closest structural homologues are the PDZ domains found in the high-temperature requirement A (HtrA) family of Ser proteases. HtrA proteases combine a protease domain to one or two PDZ domains and are involved in protein quality control[15,16]. These functions are made possible by the peptide-binding properties of PDZ domains, a domain that folds as a single β-sheet capped on one side by an α-helix, thereby delineating a groove dedicated to peptide substrates by β-strand augmentation[17].

Interestingly, the PDZ domain of MamP is unusual because its groove is not open for protein partner binding. Instead, the first visible strand in the MamP structure (β1, denoted as SP for 'self-plugging' strand) fills the binding groove found in classical PDZ domains. In MamP, this SP strand clearly contributes to its dimerization (Fig. 2a). Indeed, the position of the SP strand further allows the extension of the β-sheet, with strand β7 connecting the PDZ domain to the first magnetochrome domain. This last strand (denoted as Dim for dimerization strand) largely contributes to the dimeric interface of MamP (Fig. 2a). The overall

[1]Centre National de la Recherche Scientifique, Unité Mixte de Recherche Biologie Végétale et Microbiologie Environnementales, Laboratoire de Bioénergetique Cellulaire, Saint-Paul-lez-Durance, F-13108, France. [2]Centre National de la Recherche Scientifique, Unité Mixte de Recherche Biologie Végétale et Microbiologie Environnementales, Saint-Paul-lez-Durance, F-13108, France. [3]Aix-Marseille Université, Saint-Paul-lez-Durance, F-13108, France. [4]Synchrotron SOLEIL, L'Orme des Merisiers Saint-Aubin, 91192 Gif-sur-Yvette, France. [5]Department of Biomaterials, Max Planck Institute of Colloids and Interfaces, Science Park Golm, 14424 Potsdam, Germany. [6]Departments of Chemistry and Molecular and Cell Biology, University of California, Berkeley, Berkeley, California 94720-1460, USA. [7]Aix-Marseille Université, Laboratoire de Chimie Bactérienne, UMR7283, Institut de Microbiologie de la Méditerranée, CNRS, F-13402 Marseille Cedex 20, France. [8]Laboratoire International Associé Biomineralisation et Nanostructure, CNRS-Marseille, F-13402 Marseille Cedex 20, France. †Present address: MOH Key Laboratory of Systems Biology of Pathogens, Institute of Pathogen Biology, Chinese Academy of Medical Sciences and Peking Union Medical College, Beijing, China.

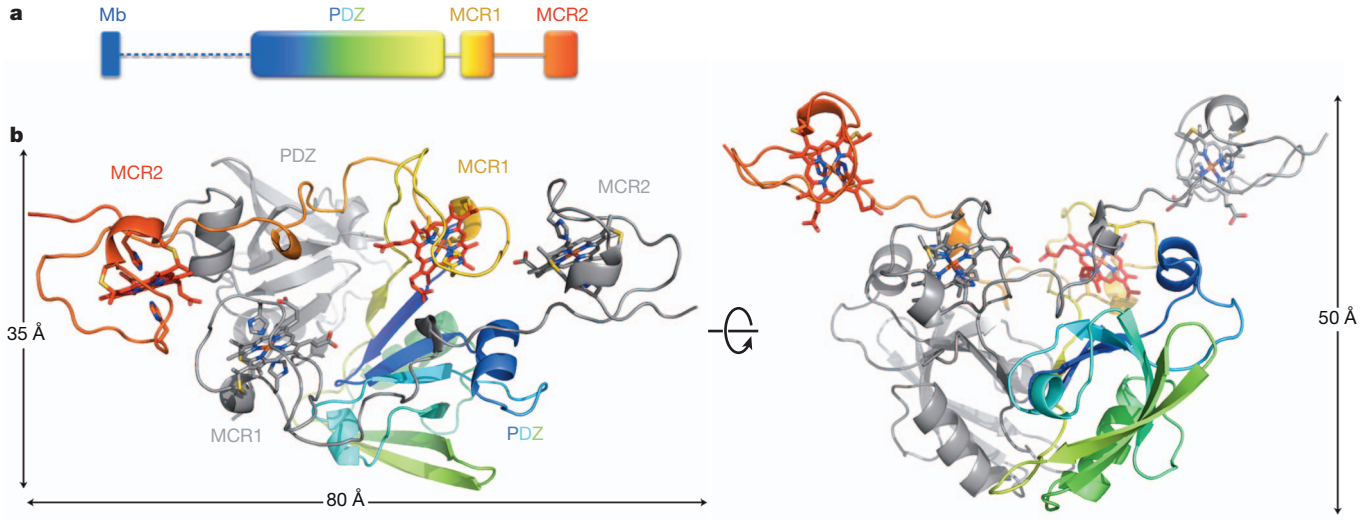

Figure 1 | Overall structure of MamP homodimer. **a**, Representation of MamP domain organization. The linker between the transmembrane helix and the PDZ domain is shown as a dashed line, indicating that it is disordered in the crystal structure. **b**, Three-dimensional structure of MamP with one monomer coloured in grey and the other monomer coloured with a ramp from blue (amino (N) terminus) to red (carboxy (C) terminus).

interface is conserved, suggesting a selective pressure for this oligomeric assembly.

We recently proposed that the two *c*-type cytochrome domains of MamP define a new domain exclusively found in MTB[10]. The present structure determination of MamP allows us to describe the fold of this domain, demonstrating its uniqueness at the structural level. A magnetochrome starts with a hydrophobic residue (ψ1 in Fig. 2b and Extended Data Fig. 2) in direct contact with the haem, followed by a Pro–His (PH) dyad, located five to nine residues upstream of the CXXCH motif, providing the sixth and fifth haem ligands, respectively. Finally, a terminal hydrophobic residue (ψ2 in Fig. 2b) closes the magnetochrome fold through a hydrophobic interaction with the ψ1 residue.

The structure of MamP also confirms that the magnetochrome domain defines a single haem-binding domain belonging to a new family of *c*-type cytochrome. Indeed, it folds as one of the smallest haem-binding units known thus far, with only 23 residues surrounding the haem (Fig. 2b). This best compares to artificial microperoxidases that possess a covalently attached haem and a single histidine ligand, whereas other mono-haem *c*-type cytochromes minimally possess about 70 residues surrounding a single haem (Protein Data Bank accession number 1K3G). We found that the haems in both magnetochrome domains are highly solvent exposed, with 281 and 214 Å^2 for MCR1 and MCR2, respectively. These values best compare to multihaem cytochromes or proteins with transient affinity for haem such as haemophores or haemopexin[18]. In addition, the haem-binding mode in magnetochrome domains also stands out because all rings of the haems are solvent exposed, which is not the case in other *c*-type cytochromes[18].

The dimeric structure of MamP creates a large surface-exposed acidic pocket resembling a crucible with approximate dimensions of 8 Å (depth) × 15 Å (diameter) (Fig. 3a). Eight conserved acidic residues from both PDZ domains delineate the bottom of this crucible, whereas the sides are formed by the propionates of the haems and four conserved acidic residues from the linkers between the two magnetochrome domains (Fig. 3a). A conserved histidine residue (H93) is located in the middle of the crucible with a network of conserved hydrogen bonded residues connecting its side chain to the exterior of the protein through polar residues, which is reminiscent of a hydrogen exit channel (Fig. 3b and Extended Data Fig. 5). The peculiar arrangement of conserved acidic residues observed in the MamP cavity suggests the presence of a 'hot spot' and led us to investigate how it reacts with iron compounds. *In vitro*, we found that MamP efficiently oxidized Fe(II)SO_4 at alkaline pH (Fig. 4a). This reaction proceeded with a rate constant (k_{ox}) of 1.06 × 10^{-3} μM^{-1} s^{-1} at an optimal pH of 9, which is comparable to observations on the multihaem cytochrome *c* MtoA, a decahaem *c*-type cytochrome from *Sideroxydans lithotrophicus* involved in microbial iron oxidation[19]. Interestingly, the optimal pH of MamP iron oxidase activity coincides with that found for *in vitro* magnetite synthesis[20].

The Fe(II) oxidation activity detected with MamP *in vitro* further prompted us to investigate whether this activity could be substantiated by structural approaches and by testing the effect of MamP on magnetite formation in solution. To get an impression of the iron oxidase activity of MamP, we transferred a MamP crystal to pH 9 and then soaked it in a solution containing Fe(II)SO_4 before data collection at the iron edge. The resulting anomalous electron density clearly indicates the presence of an iron-binding site mediated by conserved residues located at the bottom of the crucible (Fig. 4b, c). The anomalous electron density peak is only present in the open dimer and its elongated shape even suggests the presence of a di-iron-binding site with the two iron atoms replacing the two water molecules that are only seen in the high-resolution structure of the open dimer. This stabilization of two iron atoms in the open dimer is in line with the calculated charged

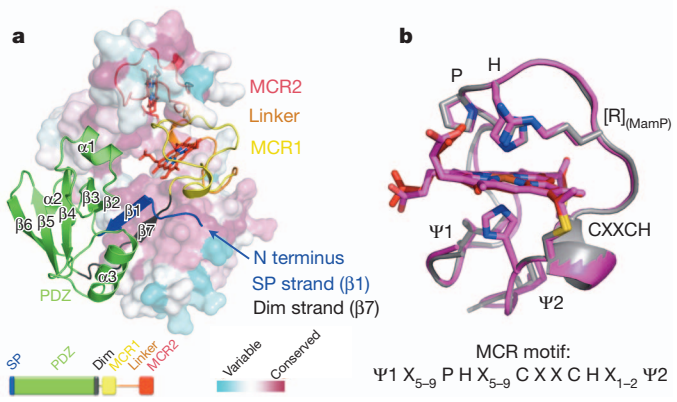

Figure 2 | A conserved dimerization interface mediated by the PDZ domain and structure of a magnetochrome domain. **a**, The surface representation of the one monomer is colour-coded based on sequence conservation in alignments of all known MamP and indicates that the dimeric interface is conserved. Note that both the self-plugged (SP) and the dimerization (Dim) strands participate in the dimerization of MamP together with strand β3 and helices α1 and α2. **b**, Superimposition of MCR1 with MCR2 with conserved magnetochrome residues represented in stick.

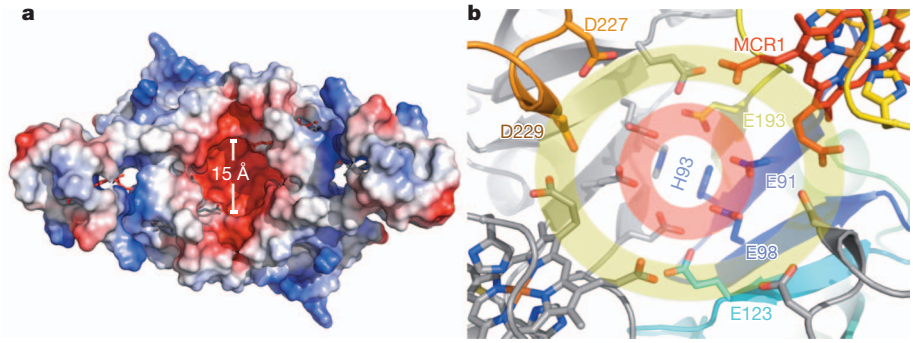

Figure 3 | A crucible on the surface of MamP is built on a conserved acidic pocket surrounded by a conserved acidic crown. **a**, Molecular surface representation of a MamP dimer coloured according to its electrostatic potential. The size of the crucible is indicated. **b**, Detail of the two acidic networks making the bottom (red circle) and the side (yellow circle) of the crucible.

states, which suggests that the iron-binding residues are unprotonated in the open dimer (Extended Data Fig. 4). Using a ferrozine assay to estimate the iron/MamP stoichiometry, we found that four irons are oxidized per MamP dimer, which provides a better fit with a di-iron-binding site.

To examine the functional relevance of the conserved acidic residues, some of which are directly involved in iron binding, we used the *mamP* deletion mutant of *Magnetospirillum magneticum* AMB-1 (the genetic tools being available for this strain), and complemented this strain with the wild-type gene or a *mamP* variant in which all conserved acidic residues are mutated to alanine (*mamP*Δ_{acid}). In accordance with our observation of an iron-binding site at the bottom of the crucible, we found that these residues are essential for magnetite formation *in vivo* as judged by the magnetic response of the cells (C_{mag}), crystal size distributions as well as transmission electron microscope (TEM) images (Fig. 4d, e and Extended Data Figs 6 and 7).

Finally, we observed the role of MamP in a mineralization experiment (Fig. 4f and Extended Data Figs 8 and 9). Indeed, magnetite is typically formed in solution by co-precipitation experiments of iron with the stoichiometric ratio of magnetite (Fe(II)/Fe(III) = 0.5) (ref. 21). We decided to start exclusively with Fe(II) to see if any mineral would form in the presence or absence of MamP. In the presence of MamP, we initially observed the formation of ferrihydrite, an Fe(III) oxide, with a progressive evolution of this mineral to magnetite (Fig. 4f). The control experiment omitting MamP could not allow the detection of any mineral by X-ray diffraction. TEM images indicated the presence of electron-dense particles that were not seen when MamP was omitted, thereby suggesting MamP-mediated production of ferrihydrite or magnetite

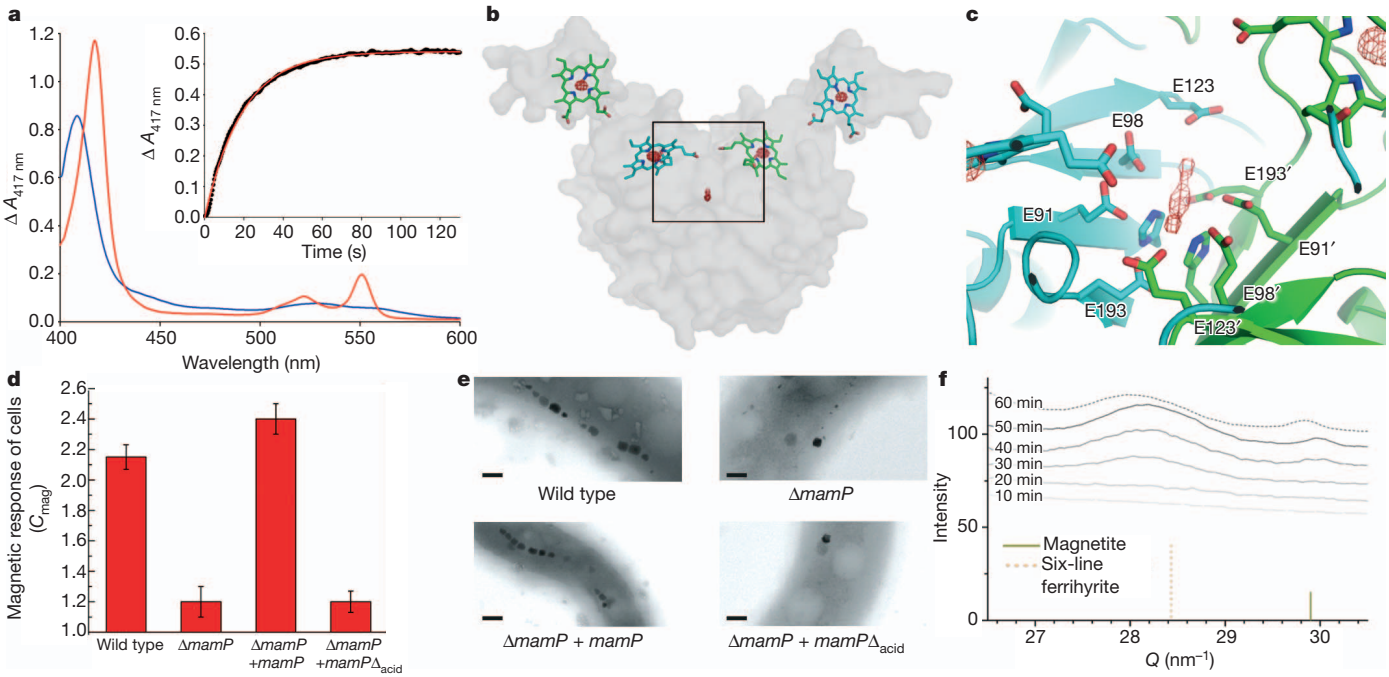

Figure 4 | MamP, an iron oxidase with a functionally important crucible, mediates ferrihydrite production in an *in vitro* mineralization experiment starting with Fe(II). **a**, Visible spectra of MamP (5 μM) before (blue line) and after (red line) addition of 50 μM Fe(II)SO_4. Inset: kinetics of reduction of MamP by Fe(II)SO_4 (black dots) and fit of the experimental data points by a single exponential (red line). **b**, Soaking experiments of MamP crystals with Fe(II)SO_4 at pH 9. The electron density map corresponds to an anomalous map collected at the iron edge and contoured at 5σ all around the dimer. **c**, Details of the position of the anomalous peak in the conserved acidic pocket. **d**, **e**, Genetic complementation studies to examine the function of MamP acidic residues. **d**, Magnetic response of cells. Data were collected as three biological replicates with two technical replicates per biological replicate. Values are represented as mean ± s.d. ($n = 6$). **e**, Representative TEM images of strains (scale bar, 0.2 μm). Cell images are representative of those collected for all three replicates. **f**, Time-resolved analysis of the mineralization synthesis followed by X-ray diffraction with reference peak of ferrihydrite and magnetite and their relative intensity (the full X-ray diffraction spectrum is shown in Extended Data Fig. 7). The six-line ferrihydrite peak ((112) peak in red dotted line) increases until 50 min whereas the magnetite peak ((400) in green) is only visible after 40 min and increases then, possibly at the expense of the ferrihydrite precursor.

(Extended Data Fig. 8). This mechanism is in accord with a process where the Fe(II) is oxidized by the protein to enable the formation of ferrihydrite, a purely ferric iron oxide. Once MamP is fully reduced, the continuous addition of Fe(II) enables the transformation of ferrihydrite to magnetite. Such a mechanism strongly resembles the pathway recently described for the synthetic formation of magnetite from solution[22].

The structural basis of MamP-mediated iron biomineralization presented here validates an old model put forth for how magnetite formation should be redox-controlled in the magnetosome, and emphasizes the versatility of the magnetochrome domains in this process[5]. Magnetite crystal growth requires a precise Fe(III)/Fe(II) ratio; the MamP properties we showed, both *in vitro* and *in crystallo*, would allow the production of the ferrihydrite precursor thanks to the presence of acidic residues at the bottom of a crucible surrounded by four magnetochrome domains. Together with the presence of iron(II), this ferrihydrite would evolve towards magnetite in the magnetosome. This molecular model fits perfectly with sequential events observed for magnetite biomineralization in MTB[6,7]. The dimension and acidic nature of the MamP crucible, the presence of a conserved proton exit channels at its bottom and the four haems on either side are well-suited for the expected chemistry of ferrihydrite formation from Fe(II):

$$4Fe^{2+} + 7H_2O \leftrightarrow (2Fe_2O_3{\cdot}H_2O) + 12H^+ + 4e^-$$

Functional and structural studies are now required to determine the contribution of other magnetochrome-containing proteins in the process of magnetite biomineralization.

METHODS SUMMARY

MamP from strain MO-1 was cloned in plasmid pET26b+ and expressed in *Escherichia coli*. The protein was purified by metal-affinity and gel-filtration chromatography. Protein crystals were obtained at 20 °C, diffraction data were collected at synchrotrons SOLEIL, SLS and ESRF, and the structure was solved by MAD. Iron oxidase activity was measured in an anaerobic glove box. We used strain AMB-1 for *in vivo* mutational analysis. *In vitro* biomineralization experiments were done under nitrogenic atmosphere using Fe(II), and X-ray diffraction was measured at synchrotron BESSY II.

Online Content Any additional Methods, Extended Data display items and Source Data are available in the online version of the paper; references unique to these sections appear only in the online paper.

Received 17 April; accepted 13 August 2013.
Published online 6 October 2013.

1. Blakemore, R. Magnetotactic bacteria. *Science* **190,** 377–379 (1975).
2. Schuler, D. Genetics and cell biology of magnetosome formation in magnetotactic bacteria. *FEMS Microbiol. Rev.* **32,** 654–672 (2008).
3. Komeili, A. Molecular mechanisms of compartmentalization and biomineralization in magnetotactic bacteria. *FEMS Microbiol. Rev.* **36,** 232–255 (2012).
4. Bell, P. E., Mills, A. L. & Herman, J. S. Biogeochemical conditions favoring magnetite formation during anaerobic iron reduction. *Appl. Environ. Microbiol.* **53,** 2610–2616 (1987).
5. Frankel, R. B. & Blakemore, R. P. Precipitation of Fe_3O_4 in magnetotactic bacteria. *Phil. Trans. R. Soc. Lond. B* **304,** 567–573 (1984).
6. Baumgartner, J. *et al.* Magnetotactic bacteria form magnetite from a phosphate-rich ferric hydroxide via nanometric ferric (hydr)oxide intermediates. *Proc. Natl Acad. Sci. USA* **110,** 14883–14888 (2013).
7. Fdez-Gubieda, M. L. *et al.* Magnetite biomineralization in *Magnetospirillum gryphiswaldense*: time-resolved magnetic and structural studies. *ACS Nano* **7,** 3297–3305 (2013).
8. Zhang, C. *et al.* Two bifunctional enzymes with ferric reduction ability play complementary roles during magnetosome synthesis in *Magnetospirillum gryphiswaldense* MSR-1. *J. Bacteriol.* **195,** 876–885 (2012).
9. Uebe, R. *et al.* The cation diffusion facilitator proteins MamB and MamM of *Magnetospirillum gryphiswaldense* have distinct and complex functions, and are involved in magnetite biomineralization and magnetosome membrane assembly. *Mol. Microbiol.* **82,** 818–835 (2011).
10. Siponen, M. I., Adryanczyk, G., Ginet, N., Arnoux, P. & Pignol, D. Magnetochrome: a *c*-type cytochrome domain specific to magnetotatic bacteria. *Biochem. Soc. Trans.* **40,** 1319–1323 (2012).
11. Lohsse, A. *et al.* Functional analysis of the magnetosome island in *Magnetospirillum gryphiswaldense*: the mamAB operon is sufficient for magnetite biomineralization. *PLoS ONE* **6,** e25561 (2011).
12. Murat, D., Quinlan, A., Vali, H. & Komeili, A. Comprehensive genetic dissection of the magnetosome gene island reveals the step-wise assembly of a prokaryotic organelle. *Proc. Natl Acad. Sci. USA* **107,** 5593–5598 (2010).
13. Quinlan, A., Murat, D., Vali, H. & Komeili, A. The HtrA/DegP family protease MamE is a bifunctional protein with roles in magnetosome protein localization and magnetite biomineralization. *Mol. Microbiol.* **80,** 1075–1087 (2011).
14. Holm, L. & Sander, C. Dali: a network tool for protein structure comparison. *Trends Biochem. Sci.* **20,** 478–480 (1995).
15. Clausen, T., Kaiser, M., Huber, R. & Ehrmann, M. HTRA proteases: regulated proteolysis in protein quality control. *Nature Rev. Mol. Cell Biol.* **12,** 152–162 (2011).
16. Krojer, T., Garrido-Franco, M., Huber, R., Ehrmann, M. & Clausen, T. Crystal structure of DegP (HtrA) reveals a new protease-chaperone machine. *Nature* **416,** 455–459 (2002).
17. Lee, H. J. & Zheng, J. J. PDZ domains and their binding partners: structure, specificity, and modification. *Cell Commun. Signal.* **8,** 8 (2010).
18. Smith, L. J., Kahraman, A. & Thornton, J. M. Heme proteins–diversity in structural characteristics, function, and folding. *Proteins* **78,** 2349–2368 (2010).
19. Liu, J. *et al.* Identification and characterization of MtoA: a decaheme *c*-type cytochrome of the neutrophilic Fe(II)-oxidizing bacterium *Sideroxydans lithotrophicus* ES-1. *Front. Microbiol* **3,** 37 (2012).
20. Baumgartner, J., Bertinetti, L., Widdrat, M., Hirt, A. M. & Faivre, D. Formation of magnetite nanoparticles at low temperature: from superparamagnetic to stable single domain particles. *PLoS ONE* **8,** 3 (2013).
21. Jolivet, J. P., Chaneac, C. & Tronc, E. Iron oxide chemistry. From molecular clusters to extended solid networks. *Chem. Commun. (Camb.)* **5,** 481–487 (2004).
22. Baumgartner, J. *et al.* Nucleation and growth of magnetite from solution. *Nature Mater.* **12,** 310–314 (2013).

Acknowledgements This work received institutional support from the Commissariat à l'Energie Atomique et aux Energies Alternatives, the Centre National de la Recherche Scientifique, Aix-Marseille University and the Max Planck Society. We are grateful to BM-30 (ESRF, Grenoble, France) and X06SA (SLS, Villigen, Switzerland) staff for technical assistance in synchrotron data collection. We thank J. Perez (SOLEIL, GIF-sur-Yvette) for help in SAXS data collection, and A. Komeili for the gift of the wild-type and Δ*mamP* AMB-1 strains. We acknowledge S. Siegel and C. Li for their support at the μSpot beamline of BESSY II, Helmholtz Zentrum Berlin. We thank the AFMB laboratory (Marseille) for circular dichroism measurements. M.I.S. was supported by a grant from the Eurotalent and ToxNuc-E programs. D.F. is supported by the Max Planck Society and a Starting Grant from the ERC (256915-MB2). S.R.J. and M.C.Y.C. thank the Defense Advanced Research Projects Agency (N66001-12-1-4230) for support.

Author Contributions M.I.S., M.W., S.R.J. and P.A. performed experiments. M.I.S., P.L. and P.A. performed structure determination. W.-J.Z. prepared genomic DNA. M.I.S., M.W., S.R.J., M.C.Y.C, D.F., P.A. and D.P. analysed the data. M.I.S., D.F., P.A. and D.P. prepared the manuscript. D.F, M.C.Y.C., P.A. and D.P. supervised the work.

Author Information Coordinates and structure factors have been deposited in the Protein Data Bank under accession numbers 4JJ0 (apo form) and 4JJ3 (in complex with iron). Reprints and permissions information is available at www.nature.com/reprints. The authors declare no competing financial interests. Readers are welcome to comment on the online version of the paper. Correspondence and requests for materials should be addressed to D.P. (david.pignol@cea.fr) or P.A. (pascal.arnoux@cea.fr).